Modeling, Simulation and Characterization of Atomic Force Microscopy Measurements for Ionic Transport and Impedance in PEM Fuel Cells

GCEP Final Report
May 5, 2008

Investigators

Peter M. Pinsky	Professor, Mechanical Engineering
David M. Barnett	Professor, Materials Science and Engineering and Mechanical Engineering
Yongxing Shen	Research Assistant, Materials Science and Engineering

Abstract

The polymer electrolyte membrane fuel cell is a power source with the potential for reducing green-house gas emissions. Characterizing the electrolyte of a fuel cell is an important procedure for assessing the performance of the entire device. The atomic force microscope (AFM) is one of the major instruments for such characterization, since it can be used for determining the surface potential and/or charge distributions in a fuel cell electrolyte. In order to understand the mechanisms involved in the AFM imaging of the membrane material, we have developed detailed models that are able to describe the contributions from sample properties and AFM probe tip geometry to the AFM images.

Electrostatic force microscopy (EFM) is an important setup of the AFM for detecting sample charge distributions. This technique, along with its variant Kelvin probe force microscopy (KPFM), records the probe-sample Coulombic interactions as the source of information in order to infer the sample charge distributions.

While electrostatic interactions are well-studied phenomena, interpreting EFM images is not a trivial problem due to the long-range nature of Coulombic interactions and the finite curvature of the probe tip. Thus, detailed modeling of this technique is demanded for quantitative analysis of such images, which we have approached from two opposite directions.

In the forward problem, we assume complete knowledge of the sample (in this case the fuel cell electrolyte), the instrument, and the imaging mechanism and aim to predict the image. For very general configurations, we have used the boundary element method to solve this well-posed boundary value problem and developed post-processing procedures to predict measurable quantities (e.g., tip-sample interaction force and its gradient with respect to the tip motion). From the solution to the forward problem, we have gained insights about the tip-sample interactions and the image sensitivity to variations in sample properties (e.g., work function variation), probe geometries (e.g., tip radius of curvature) and experimental conditions (e.g., tip-sample spacing).

On the other hand, the inverse problem is concerned with determining sample properties of interest (in this case, fuel cell electrolyte charge distributions) from the images obtained from experiments. This is an ill-posed problem due to non-uniqueness and instability. In the case of a flat dielectric sample, we have established a convolution relation between sample trapped charge distributions and the corresponding KPFM images. With this relation, we have developed a deconvolution algorithm to solve for the desired sample charge distributions and applied it to experimentally obtained images on fuel cell electrolyte materials.

Introduction

Invented in 1986 [1], the atomic force microscope (AFM) has been and continues to be a prominent instrument for imaging and characterizing the surfaces of fuel cell electrolyte materials. Such imaging is absolutely essential for understanding why certain designs, selections, and processing of fuel cell membrane materials prove to be successful or unsuccessful choices. In this sense the AFM is currently as crucial to fuel cell technology development as is imaging by electromagnetic and other radiation in modern medicine and health care.

The key part of the AFM is a conical probe tip attached to the free end of a cantilever, as shown in Figure 1. As the probe scans a sample of interest, the AFM is able to produce images by recording the variation of some quantities related to the probe-sample interaction, e.g., the deflection or the oscillation amplitude of the cantilever. These images provide information about the fuel cell electrolyte, e.g. the surface topography and the charge distribution.

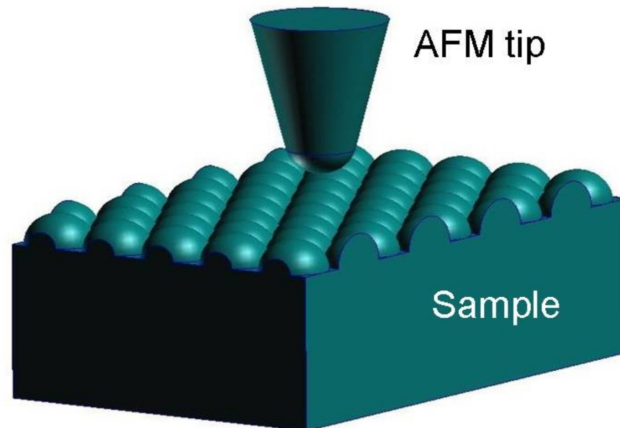

Figure 1: Schematic of the AFM tip (without the cantilever) and the sample

Of the existing experimental configurations of the AFM, electrostatic force microscopy (EFM) [2] and related techniques (e.g., Kelvin probe force microscopy (KPFM) [3] and scanning capacitance microscopy (SCM) [4]) use the Coulombic interaction between the AFM probe and the sample of interest as the source of information to generate images. These techniques can detect the existence and distribution of fuel cell charges. In order to separate the long-range electrostatic force from the short-range forces, such as van der

Waals interaction and chemical bonding, the experiment requires a certain separation between the probe tip and the sample, ranging from 2 nm to 100 nm; hence, these techniques are categorized as *non-contact* atomic force microscopy.

As noted above, interpreting EFM images is a non-trivial problem due to the long-range nature of Coulombic interactions and the finite curvature of the probe tip. Detailed modeling of this technique is required for quantitative analysis of images and our approaches are described in the next section.

Background

A number of models describing probe-sample interactions have been proposed in the last two decades. Earlier models assumed the sample to be a semi-infinite conductor with a flat surface, which permitted the use of the image charge method. Within this framework, some models treated the probe surface as an equipotential with an assumed distribution of charges, such as a single point charge [6] or a uniformly charged line [7], and the probe-sample interaction was approximated as the interaction between the assumed charge distribution and its image with respect to the sample surface. Another group of models introduced geometric approximations to the probe shape and solved the probe-sample capacitance problem either by exactly solving the boundary value problem, e.g., the sphere model [8] and the hyperboloid model [9], or by introducing further approximations to the electric field between the probe and the sample [10-12]. These models provide convenient analytic expressions of the probe-sample interaction; however, more sophisticated models are demanded for studying the lateral variation of the sample surface properties (e.g., topography and trapped charge distribution) and the associated EFM measurements.

This demand has attracted researchers to attack the problem from different perspectives. Their models may be grouped into three families according to their methodologies. One family of models invoked the molecular dynamics (MD) technique to track the motion of the atoms of the probe tip and the sample surface, while modeled the cantilever as a point mass to take into account its oscillation [13,14]. This model captured detailed atomic configurations of both solids and provided atomic-level information of the probe-sample interactions, including both Coulombic and van der Waals forces, and hence required reasonable initial conditions. And as for general MD systems, numerical artifacts were introduced to these models by the use of periodic boundary conditions.

A second family of models replaced the probe and the sample by a series of point charges and/or line charges and their image charges [15, 16]. Based on this method, interactions between the probe and a conductive or dielectric sample with topographic and/or dielectric in homogeneities [17-19] have been studied. This approach was capable of accommodating different scenarios, but the selection of source and test points may suffer from arbitrariness and might lack consistency between different selections.

The third family of approaches solved the well-defined electrostatic boundary value problem using continuum-level numerical schemes such as the finite element method [20], the self-consistent integral equation method [21], the multiple multipole program

[22], and the boundary element method [23]. References [22] and [23] also provided de-convolution algorithms for conductive samples to reconstruct the tip-sample contact potential difference (CPD) from a KPFM measurement which the authors proved to be a convolution of the probe geometry and the CPD.

Of these models, the boundary element method proposed by Strassburg et al. [23] possesses advantages over other methods for modeling EFM in some important aspects. First, the EFM probe tip geometry can be exactly taken into account up to the discretization error, which permits comparison of different probe tip shapes. Second, no truncation is required for the vacuum domain (the space outside the probe and the sample) which has an infinite dimension but a uniform dielectric constant. Third, only surface discretization is required to solve the electrostatic problem; hence, there are fewer unknowns in the formulation than domain based techniques such as the finite element. For the case of a topographically flat sample, this reduction is even more pronounced,

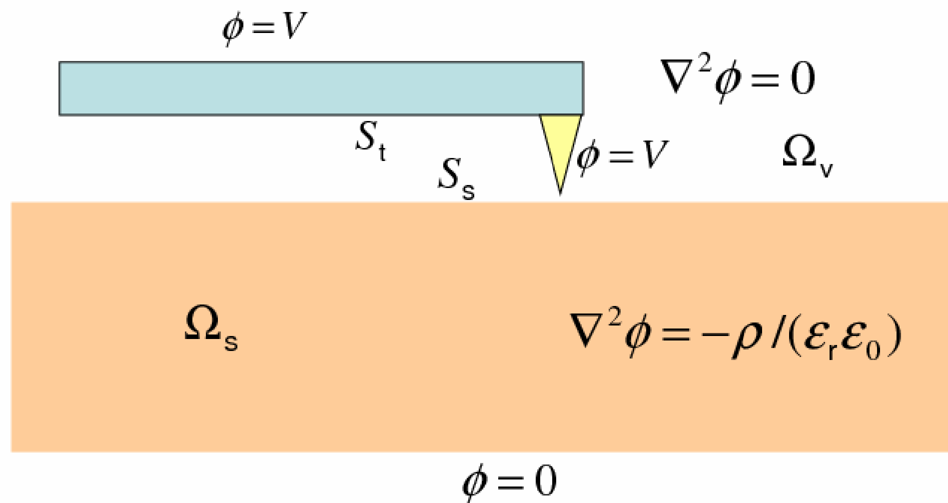

Figure 2: Schematic of the electrostatic boundary value problem involved in EFM/KPFM.

because the sample surface can be described using the image charge method and hence only the probe surface needs discretization.

Results

We have approached the problem of modeling EFM/KPFM studies on fuel cell electrolyte materials from two opposite directions: forward problem and inverse problem.

Forward problem modeling: predicting measurements (Project publications P1, P3, P4, P5)

For the forward problem, we have started with the boundary value problem (see Figure 2) that describes the probe-sample interaction and transform it to the equivalent boundary integral equation in order to solve for the electric field and predict the KPFM signal.

As a consequence of the dimensions of the problem, we are justified in applying a quasistatic approximation despite the time dependent voltage applied between the probe tip and the sample. This approximation allows us to neglect the magnetic field. The KPFM cantilever with the probe tip is assumed to be a perfect conductor, whose potential is a constant. The sample is assumed to be semi-infinite with a flat surface and an isotropic homogeneous dielectric constant. A conductive sample can be treated as a special case in which the dielectric constant tends to infinity.

The electrostatics involved in KPFM is described by Poisson's equation in the sample interior and Laplace's equation in the open space (vacuum) outside the probe tip and the sample.

The boundary value problem is a two-domain problem with a Dirichlet boundary condition on the surface of the cantilever plus the probe tip and two continuity conditions across the sample surface involving the sample surface dipole layer (double layer) density and charge (single layer) density.

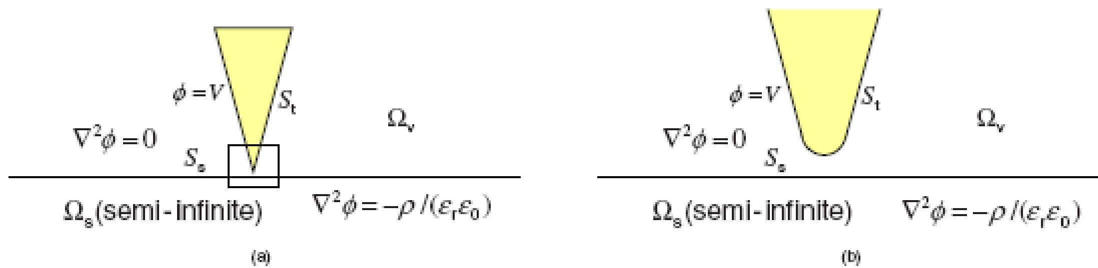

Figure 3: (a) Schematic of the electrostatic boundary value roblem simplified by (i) neglecting the cantilever and (ii) assuming the sample to be semi-infinite. (b) Magnification of a region of (a) in proximity to the tip apex [*schematically* shown in a box in (a)].

If the sample surface is flat, a boundary integral equation equivalent to this boundary value problem can be derived from Green's second identity, taking into account the contributions to the electric field by the sample surface charges, surface dipoles, and interior charges. The primary unknown of this boundary integral equation is the induced surface charge density on the probe tip. After this induced surface charge density has been solved, the total force exerted on the probe tip can be obtained by integrating over the probe tip surface the traction associated with the Maxwell stress tensor.

As a result of their large distance from the sample--and thus the electrostatic forces they exert thereupon--and for the sake of simplicity, only the tip apex and the conical portion of the probe is included in the numerical treatment while the cantilever is neglected, as shown in Figure 3(a) (The tip apex radius of curvature, the cone height, and the cantilever length are on the orders of 40 nm, 15 μm, and 100 μm, respectively). A magnification for the region in proximity to the tip apex is shown in Figure 3(b).

For the first set of examples for the forward problem solution, we choose two dielectric samples, each of which contains a surface dipole layer of 1 V over a square and 0

otherwise, as shown in Figures 4(a) and 4(c). The side of the square in Figure 3(a) is 1.75 times the tip radius of curvature, whereas that of the square in Figure 3(c) is 17.5 times (i.e., one order larger than) the tip radius of curvature. In addition, these samples are assumed to have no other sources to interact with the probe. Hence, the surface potentials measured by KPFM, VKPFM, especially the second one, are expected to be faithful to the true potential.

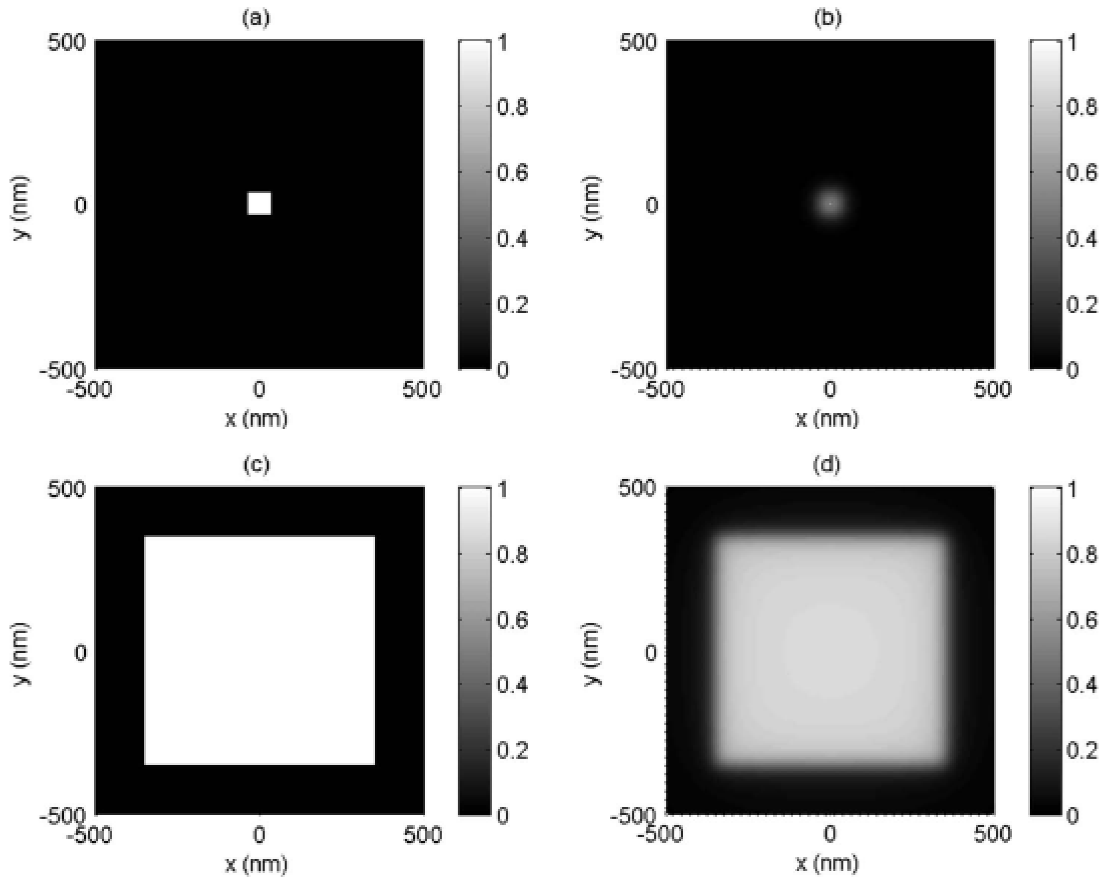

Figure 4: [(a) and (c)] Prescribed surface dipole density (true surface potential) Φ of samples with a dielectric constant of 30.0 with no trapped charge distributions. Φ = 1 V over a square centered at (0, 0) with a side of (a) 70 nm, or (c) 700 nm, and 0 otherwise. [(b) and (d)] Predicted KPFM image of these samples. The KPFM probe tip radius of curvature is taken to be 40 nm, the tip total length is 15 μm, the tip half conical angle is 15°, and the tip-sample separation is 15 nm. The maximum predicted KPFM measurement [the value at (0,0)] are (b) 0.46 V and (d) 0.85 V, so that the minimum pointwise errors of the surface potential are 54% and 15%, respectively. Components of the discrete dipole response function can be inferred from the pixel intensities of the predicted image (b).

The predicted KPFM images are shown in Figures 4(b) and 4(d). The shapes of the "measured" potential inhomogeneity do resemble the true surface potential; however, the measured potential values differ from the true values by *at least* 54% and 15% for these two cases. This can be attributed to the long-range characteristic of the Coulombic force, the consequence of which is that the portion of the sample surface outside the square also participates significantly in the interaction with the probe tip. As a result, the KPFM is registering a *weighted average* of the sample surface potential (in this case, weighted averages of 1 and 0 V), leading to this instrumental error.

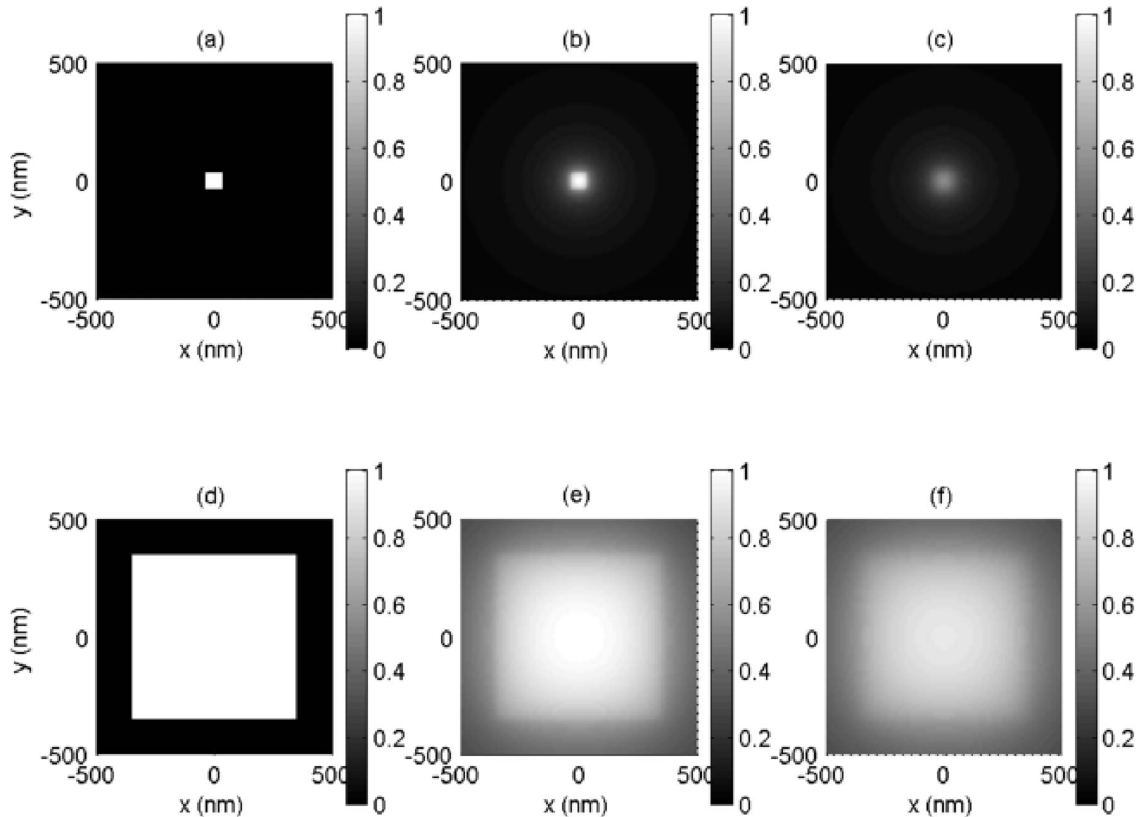

Figure 5: [(a) and (d)] Contour plots of prescribed surface charge densities Σ with supports as pixels with dimensions Δ, where Δ=70 nm and 700 nm, respectively. For each case, Σ equals some positive constant over the square and 0 otherwise. [(b) and (e)] The single layer potentials on the sample surface due to the charges in (a) and (d). In both cases, the tip is *absent*. The potentials are normalized so that the maximum values are 1 V. [(c) and (f)] Predicted KPFM images due to charges described in (a) and (d), respectively. The experimental setup and the sample property are the same as those in Figure 3. The potential values at the centers of the squares of (c) and (f) are 0.55 and 0.90 V, respectively. Components of the discrete dipole response function can be inferred from the pixel intensities of the predicted image (b).

In the second set of examples, we choose dielectric samples containing a surface charge layer, as shown in Figures 5(a) and 5(d), where the sizes of the charged areas are the same as those in Figures 4(a) and 4(c), respectively. The single layer potentials on the surfaces due to these charges in the *absence* of any instrument (literally surface potential) are plotted in Figures 5(b) and 5(e), respectively, which are assumed to be what an *ideal* instrument would register. The predicted KPFM images are shown in Figures 5(c) and 5(f), from which one can also see the broadening effect for small areas of charges; moreover, the errors of KPFM-measured potential values (referenced to the surface potentials) at the centers are also as large as 45% and 10%, respectively.

From the results of the forward problem study, we have found that inverse algorithms are needed for interpreting KPFM images due to the convolution effect. The KPFM image is the sum of the contributions from the sample surface dipole, surface charge, and interior charge. The contribution from each type of sources is a convolution of the actual source and the corresponding response function.

Inverse problem modeling: analyzing images (Project Publications P3, P6)

While the forward problem of predicting KPFM images from dielectric sample properties is a classical potential problem, solving the responsible sample properties from such images is an inverse problem with insufficient data. The primary insufficiency comes from the fact that for a particular sample, the surface dipole, the surface trapped charge, and the interior trapped charge contribute to the overall Coulombic interaction simultaneously, and their contributions are difficult to isolate from one another. As a result, without further information there will be no unique solution given a particular image.

To overcome this difficulty, one needs a more detailed description of the sample properties in order to deduce more equations or fewer unknowns. For example, the interior charge contribution to the image can be absorbed in the surface charge contribution term by assuming that the detectable charges are distributed close to the surface. The justification is that KPFM, being a *surface* characterization technique, is usually not expected to be able to register the charge variations *inside* the sample due to the unavoidable thermal noises.

Another aspect of incompleteness comes from the fact that only a *subset* of the sample surface is imaged, but sources (charges/dipoles) outside the imaging area also contribute to the overall Coulombic interaction. This incompleteness is overcome when we implicitly introduce the assumption of a periodic source in order to perform the discrete Fourier transform.

If the sample of interest can be modeled as having either only a surface dipole layer distribution or only a surface charge layer distribution that is responsible for the Coulombic interaction with the probe tip, then there remains only one unknown field, and the convolution relation becomes a one-to-one mapping from the source to the image, allowing one to solve for the source from the image via deconvolution. Such a deconvolution algorithm was first proposed by Strassburg et al. [23] to solve for the

surface potential variations of flat conductive samples. They implemented it for the special case of one-dimensional surface potential variation, i.e., the case in which the surface potential is a function of only one Cartesian coordinate. We have generalized this algorithm for dielectric samples and performed, for the first time, a two-dimensional deconvolution study on a KPFM image to solve for the sample's surface charge density.

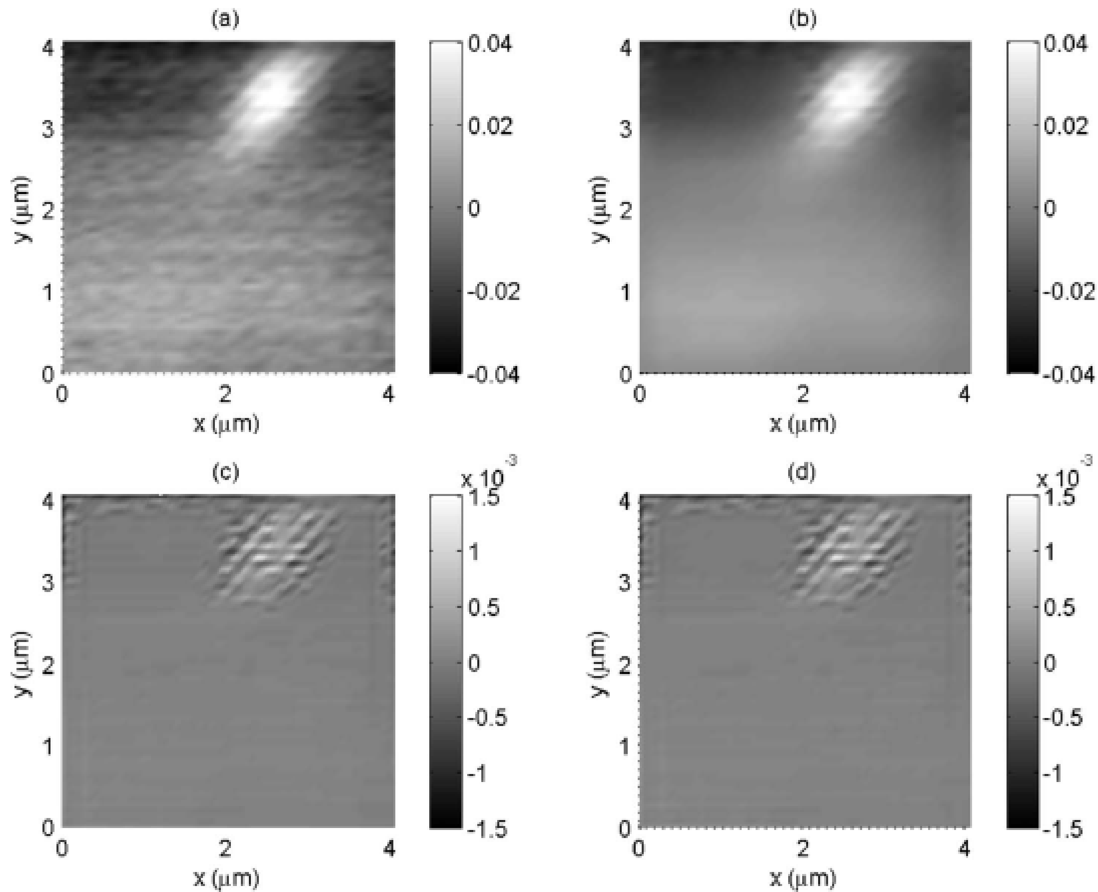

Figure 6: (a) Raw [24] and (b) noise-filtered (with the Wiener filter) KPFM images on a gadolinia-doped ceria thin film. The units of both are V. The probe is 15 μm long and has a half conical angle of 15°. The probe tip radius is 40 nm. The tip-sample separation is 15 nm. The dielectric constant is 30.0. The spacing of the sampling points is 70 nm. The number of sampling points in either direction is 59. [(c) and (d)] Contour plots of the reconstructed surface charge density from (b) via deconvolution. The unit is e/nm^2, where e is the elementary charge. Before deconvolution, the filtered data are extended with zeros to render (c) 128 x 128 or (d) 256 x 256 data points to mitigate the edge effect. The discrete response functions are arrays of the respective sizes.

We have applied the deconvolution algorithm for a KPFM image obtained by Lee [24] from experiments shown in Figure 6(a). The sample is a gadolinia-doped ceria (GDC) [note: we are using *solid oxide* fuel cell electrolyte materials as our model materials since their charge distributions are better known compared to *polymer electrolytes*; however, our formulation and numerical scheme also apply to polymer electrolytes] thin film which is a popular material used as electrolyte in solid oxide fuel cells. This thin film has a thickness of 50–100 nm. It was fabricated by sputtering $Gd_{0.2}Ce_{0.8}$ alloy (Kurt Lesker Co.) on a 200 nm thick Pt layer (serving as a reference electrode), which had been sputtered on a silicon nitride film. The $Gd_{0.2}Ce_{0.8}$ film was then oxidized in air at 650 °C for 5 hours.

The surface modulation, topographic measurement, and the surface potential measurement on the GDC film were performed in ambient condition at room temperature using the same instrument, Molecular Imaging Inc.'s PicoPlus II AFM with a probe coated with highly boron-doped diamond. In addition, commercial radio frequency lock-in amplifiers with dedicated circuitry were set up for imaging the surface potential.

Before being imaged, the sample surface was modulated by placing the probe tip *in contact* with the sample and applying a positive dc voltage on the tip (referenced to the Pt layer) to facilitate some chemical reaction. After that, the topography and the surface potential were measured in the contact mode and the amplitude modulation mode, respectively. Such measurements were performed for each scan line to generate maps of topography and surface potential.

As a result of the surface modulation, a peak centered at the former contact region is observed in the subsequent KPFM image, indicating charge concentration in this region compared to the rest of the imaging area. We have used our deconvolution algorithm to obtain the surface charge density from the KPFM image. To reduce the noise, we have applied the Wiener filter to the image prior to other numerical treatment. Figure 6(b) shows the Wiener-filtered image. To mitigate the edge effect, we have extended the image with zeros. After that, the deconvolution algorithm leads to the solution of surface charge densities shown in Figures 6(c) and 6(d), with a different choice of a parameter.

From Figures 6(c) and 6(d), we can see that the Gaussian-like intensity variations in Figure 6(a) become localized sources in Figures 6(c) and 6(d). The surface charge densities shown in Figures 6(c) and 6(d) are solutions to the inverse problem, which are more appropriate descriptions for samples of this kind compared to the raw image with (broadened) "CPD" values ill defined for dielectric samples.

Conclusions

We have developed a theoretical framework to model electrostatic force microscopy (EFM) measurements on conductive and dielectric samples, in particular, on fuel cell electrolyte materials. The boundary element method proves to be an efficient numerical method for predicting EFM measurements based on prescribed sample properties and probe tip geometry. Based on this framework, inverse algorithms can be developed to solve for the desired sample charge distributions from images obtained from experiments.

Such results help assess the quality of a certain design of fuel cell and are able to improve the current fuel cell technology, leading to a better prospect of zero-emission power sources.

Project Publications

P1 Shen, Y., D. M. Barnett, and P. M. Pinsky, Modeling electrostatic force microscopy for conductive and dielectric samples using the boundary element method: Eng. Anal. Bound. Elem., accepted for publication, doi:10.1016/j.enganabound.2007.12.003.

P2 Shen, Y., D. M. Barnett, and P. M. Pinsky, Analytic perturbation solution to the capacitance system between a hyberboloidal tip and a rough surface: Appl. Phys. Lett., 92, 134105, 2008.

P3 Shen, Y., D. M. Barnett, and P. M. Pinsky, Simulating and interpreting Kelvin probe force microscopy images on dielectrics with boundary integral equations: Rev. Sci. Instrum., 79, 023711, 2008.

P4 Shen, Y., M. Lee, W. Lee, D. M. Barnett, P. M. Pinsky, and F. B. Prinz, A resolution study for electrostatic force microscopy on bimetallic samples using the boundary element method: Nanotechnology, 19, 035710, 2008.

P5 Shen, Y., D. M. Barnett, and P. M. Pinsky, Integral equation modeling of electrostatic interactions in atomic force microscopy. In: C. Constanda and S. Potapenko (eds.), Integral Methods in Science and Engineering: Techniques and Applications, Birkhäuser, Boston, 237-246, 2007.

P6 Shen, Y., D. M. Barnett, and P. M. Pinsky, Determining charge distributions from Kelvin probe force microscopy images: Ninth US National Congress on Computational Mechanics, San Francisco, California, 2007.

P7 Shen, Y., D. M. Barnett, and P. M. Pinsky, Integral equation modeling of electrostatic interaction in atomic force microscopy: Ninth International Conference on Integral Methods in Science and Engineering, Niagara Falls, Ontario, Canada, 2006.

P8 Shen, Y., D. M. Barnett, and P. M. Pinsky, Quantitative modeling of electrostatic force microscopy: Materials Research Society Fall Meeting, Boston, Massachusetts, 2005.

References

1. Binnig, G., Quate, C.F., and Gerber, Ch., Atomic force microscope, Phys. Rev. Lett., 56, 930-933, 1986.
2. Stern, J.E., Terris, B.D., Mamin, H.J., and Rugar, D., Deposition and imaging of localized charge on insulator surfaces using a force microscope, Appl. Phys. Lett., 53, 2717-2719, 1988.
3. Nonnenmacher, M., O'Boyle, M.P., and Wickramasinghe, H.K., Kelvin probe force microscopy, Appl. Phys. Lett., 58, 2921-2923, 1991.
4. Williams, C.C., Hough, W.P., and Rishton, S.A., Scanning capacitance microscopy on a 25 nm scale, Appl. Phys. Lett., 55, 203-205, 1989.
5. Girard P., Electrostatic force microscopy: principles and some applications to semiconductors, Nanotechnology, 12, 485-490, 2001.
6. Hu, J., Xiao, X.-D., Ogletree, D.F., and Salmerón, M., Imaging the condensation and evaporation of molecularly thin films of water with nanometer resolution, Science, 268, 267-269, 1995.
7. Hao, H.W., Baró, A.M., and Sáenz, J.J., Electrostatic and contact forces in force microscopy, J. Vac. Sci. Technol. B, 9(2), 1323-1328, 1991.
8. Terris, B.D., Stern, J.E., Rugar, D., and Mamin, H.J., Contact electrification using force microscopy, Phys. Rev. Lett., 63 (24), 2669-2672, 1989.
9. Pan, L.H., Sullivan, T.E., Peridier, V.J., Cutler, P.H., and Miskovsky, N.M., Three-dimensional electrostatic potential, and potential-energy barrier, near a tip-base junction, Appl. Phys. Lett., 65, 2151-2153, 1994.
10. Hochwitz, T., Henning, A.K., Levey, C., Daghlian, C., and Slinkman, J., Capacitive effects on quantitative dopant profiling with scanned electrostatic force microscopes, J. Vac. Sci. Technol. B, 14, 457-462, 1996.

11. Hudlet, S., Saint Jean, M., Guthmann, C., and Berger, J., Evaluation of the capacitive force between an atomic force microscopy tip and a metallic surface, Eur. Phys. J. B, 2, 5-10, 1998.
12. Colchero, J., Gil, A., and Baró, A. M., Resolution enhancement and improved data interpretation in electrostatic force microscopy, Phys. Rev. B, 64, 245403, 2001.
13. Livshits, A.I., Shluger, A.L., Rohl, A.L., and Foster, A.S., Model of noncontact scanning force microscopy on ionic surfaces, Phys. Rev. B, 59, 2436-2448, 1999.
14. Barth, C., Foster, A.S., Reichling, M., and Shluger, A.L., Contrast formation in atomic resolution scanning force microscopy on CaF_2(111): experiment and theory, J. Phys.: Condens. Matter, 13, 2061-2079, 2001.
15. Mesa, G., Dobado-Fuentes, E., and Sáenz, J.J., Image charge method for electrostatic calculations in field-emission diodes, J. Appl. Phys., 79, 39-44, 1996.
16. Belaidi, S., Girard, P., and Leveque, G., Electrostatic forces acting on the tip in atomic force microscopy: Modelization and comparison with analytic expressions, J. Appl. Phys., 81 (3), 1023-1030, 1997.
17. Gómez-Moñivas, S., and Sáenz, J.J., Theory of electrostatic probe microscopy: A simple perturbative approach, Appl. Phys. Lett., 76, 2955-2957, 2000.
18. Gómez-Moñivas, S., Froufe-Pérez, L., Caamaño, A.J., and Sáenz, J.J., Electrostatic force between sharp tips and metallic and dielectric samples, Appl. Phys. Lett., 79, 4048-4050, 2001.
19. Sacha G.M., Gómez-Navarro, C., Sáenz, J.J., and Gómez-Herrero, J., Quantitative theory for the imaging of conducting objects in electrostatic force microscopy, Appl. Phys. Lett., 89, 173122, 2006.
20. Belaidi, S., Lebon, E., Girard, P., Leveque, G., and Pagano, S., Finite element simulations of the resolution in electrostatic force microscopy, Appl. Phys. A, 66, S239-S243, 1998.
21. Li, Z.-Y., Gu, B.-Y., and Yang, G.-Z., Scanning-electrostatic-force microscopy: Self-consistent method for mesoscopic surface structures, Phys. Rev. B, 57, 9225-9233, 1998.
22. Jacobs, H.O., Leuchtmann, P., Homan, O.J., and Stemmer, A., Resolution and contrast in Kelvin probe force microscopy, J. Appl. Phys., 84, 1168-1173, 1998.
23. Strassburg, E., Boag, A., and Rosenwaks, Y., Reconstruction of electrostatic force microscopy images, Rev. Sci. Instrum., 76, 083705, 2005.
24. Lee, M., PhD thesis, Stanford University, in preparation.

Contact Information

Peter M. Pinsky: pinsky@stanford.edu
David M. Barnett: barnett@stanford.edu